

Chapter

Delamination and Tensile Effect of Fine z-Binder Reinforced on Fiberglass/Polyester Composite for Aerospace Applications

Citlalli Gaona-Tiburcio, Alejandro Lira-Martínez, Marianggy Gomez-Avila, Jesús M. Jaquez-Muñoz, Miguel Angel Baltazar-Zamora, Laura Landa-Ruiz, Demetrio Nieves-Mendoza, Francisco Estupiñan-López and Facundo Almeraya-Calderón

Abstract

Delamination propagation in laminated composite materials is a common issue that always concerns us when we consider composites for structural purpose. Many possible solutions have been studied; the most famous is the three-dimensional (3D) woven composites materials, which have promising interlaminar fracture resistance but at the cost of increasing density, which for aerospace industry is very important. In this chapter, mode 1 double cantilever beam (DCB) interlaminar fracture toughness tests according to the American Society for Testing and Materials (ASTM) D5528 standard were performed on composite specimens made of E-Glass Saertex 830 g/m² Biaxial (+/-45°) with Sypol 8086 CCP polyester resin with orthogonal z-axis oriented yarn woven of 0.22 mm diameter nylon monofilament. Four specimens were made with a longitudinal distance between the warp binders of 0.5, 1, 1.5, and 2 cm, respectively. A tensile test according to the ASTM D3039 standard was performed to study how z-binder may affect tensile resistance. The results show a considerable increase in interlaminar fracture toughness, several stress concentrators have been created because of the new yarn and premature failure in the matrix.

Keywords: composite, delamination, laminated, tensile, interlaminar

1. Introduction

A composite material, from now on just “composites,” consists of 3 components known as reinforcement, matrix, and the interface between whose properties and performance are designed so that together they generate material with superior

properties to its parts acting independently. In general, the “Reinforcement” is a very rigid and strong material with a distributed phase, whose function is to support the external forces in its longitudinal direction.

At the same time, the “matrix” is a material with a continuous phase, weaker, and less rigid, but more tenacious and often more chemically inert, which is responsible for keeping the reinforcement attached to the final shape of the mold in which it is located, protecting the reinforcement against external agents, supporting indirect stresses along the length of the reinforcement and helping to distribute external mechanical energy to the reinforcement, so that it be distributed and supported by the latter. The “interface” is created as the chemical interaction and bonding between reinforcement and matrix. From here, the composites are classified due to (a) the shape of the reinforcement, such as continuous or discontinuous fibers, particles, etc., and (b) the nature of the matrix, which can be a metallic, ceramic, or polymeric matrix. When composites are manufactured as a set of layers or laminates, it is simply known as laminate composites [1].

The use of composites in the aerospace industry has grown rapidly from the mid-1990s to the present, so now, it is one of the most used materials in commercial aircraft. This interest and investment in composites are because, in many cases, their properties are generally better than those of metals, especially aluminum alloys, such as lower density, better mechanical properties, they do not corrode, and with a proper design, manufacturing costs can be reduced by reducing solid joint elements such as rivets [2].

Unfortunately, laminate composites have several disadvantages over metals. One of the most important issues is delamination, a critical failure mechanism caused by high interlaminar stresses coupled with typically very low through-thickness strength. Delamination arises because fibers lying in the plane of a laminate do not provide through-thickness reinforcement, so the composite transfers most of the external load into the matrix, which usually is quite brittle and very susceptible to shear stress, so that the laminate composite starts to separate between laminates, as illustrated in **Figure 1** [3].

Specifically speaking of fiberglass/polyester composites, there are some works that report studies on their manufacture, composition, and properties, but also another more specific that analyzes thermal properties, crack growth behavior, fracture energy, the effect of mode of loading, and delamination resistance.



Figure 1.
Composite delamination.

Bagherpour [4] published a book in which he analyzes the mechanical relationships in fiber-reinforced polyester composites. He explains its tensile, bending, and toughness properties.

Gupta [5] investigated the water absorption and thermal and mechanical properties of glass fiber reinforced polymeric composites, finding that all of them increase with the increasing number of glass fiber layers. Ganjani [6] in 2021 considered the effect of mode II delamination and the corresponding interlaminar crack propagation during the drilling process of multilayer glass/polyester composites, using numerical and experimental approaches; and found that more than 95% of the crack propagation could be attributed to mode II under the conditions studied.

Triki [7] in his research on the influence of the fabric structure on the crack growth behavior of glass/polyester composite laminates, using fracture toughness tests, was able to determine that the balanced interface is more resistant to delamination than the unbalanced interface.

Sham [8] published a review in which she highlights aspects of interlaminar and intralaminar fracture toughness studies of polymeric matrix composites and lists the different ways to assess fracture energy.

Khoramshahi [9] investigated both experimentally and numerically, the effect of mixed-mode loading on the fracture parameters of glass-reinforced polyester composite specimens, and according to the measured fracture toughness, they found the energy release rates of critical interlaminar deformation in opening and shear mode. Furthermore, her results indicated that the interlaminar cracked sample is stronger under shear loading conditions and weaker under tensile loading conditions.

More recently, Suriani [10] published a review in which she compiles other works on delamination and some common types of manufacturing defects, thereby illustrating the impact on mechanical properties and proposing alternative solutions.

Various investigations have been done on delamination due to through-thickness stresses [11–21]. However, it has been widely neglected that delamination also has a crucial role in determining in-plane strength, often leading to premature failure initiation. In-plane failure of composites is driven by the energy released when the fibers are discharged. This can occur in two ways: by fracture of the fibers or by delamination and cracks in the matrix that come together to produce a fracture in the surface without breaking the fibers. Delamination also plays a critical role in the behavior of composites under the impact, affecting both the damage caused under impact load and the subsequent response in compression after the impact [3].

Currently, four types of delamination are defined as fracture mechanisms classified by modes, and mode I is the one studied in this chapter, in which the normal stresses are produced perpendicular to the interlaminar crack, and the surfaces of the separate crack one from the other without there being any relative slippage of them; it is shown in **Figure 1** [22]. There are some interesting investigations about the mode-I delamination process, the effect of the reinforcement, and the Z-fiber or Z-pinned laminates, mainly using carbon fiber or epoxy [23, 24].

Many applications in aircraft parts are exposed to out-of-plane loading conditions that make it impossible to turn laminated composites into a proper material. Wind turbine blades, aircraft spars, stiffeners, and pressure vessels are examples of applications where out-of-plane loading conditions are imposed on the structure. Therefore, a delamination solution has arisen as a composite with improved full-thickness “out-of-plane” properties, known as a 3D woven composite [25].

Conventionally the reinforcement used for laminated composites is a 2-dimensional (2D) fabric; therefore, it is impossible to protect the matrix from trough

thickness stresses. The three-dimensional (3D) reinforcement for composites contains a fabric that covers the 3 dimensions (length, width, and thickness) and is a technology that is having great success in the aerospace industry, such as the very know composite blades from LEAP turbofan, which is a generation of the CFM56 Aerojet produced by CFM (Snecma and GE) and SAFRAN [26].

This chapter is the characterization of stress fracture and Mode 1 delamination in laminated composites reinforced in cross section with a 3D fabric whose objective is the application in aeronautical structures. The transverse reinforcement was made using an industrial sewing machine as part of an external company project, and a 0.5 mm diameter thread was used. The study variable in the reinforcement was the space between reinforcement and longitudinal reinforcement to the composite, having reinforcements with a distance of 2, 1.5, 1, and 0.5 cm, respectively. The reinforced composite was manufactured, and a tensile test was carried out according to the ASTM D3039 standard [27]. Mode 1 of delamination analysis was carried out according to the ASTM D5528 standard to characterize tensile strength and its resistance to delamination [28]. Results were compared with z-axis binder and without binder, and the failures were characterized by fractographic analysis using a stereoscope. The purpose of the separation between the reinforcement is to find a possible variation in the resistance to delamination of the material since the more intertwined between the warp and weft, the greater the probability of generating stress concentrators and, therefore, reducing its interlaminar resistance. This new material is meant to be used in aircraft's control surfaces, several sources [29–32] report various issues regarding delamination on such surfaces, which is one of the most predominant uses of this kind of material.

2. Experimental procedure

The specimens were performed according to ASTM D5528 standard by resin transfer molding (RTM) process with E-Glass Saertex 830 g/m² Biaxial (+/-45°) through-the-thickness (TTT) binder by an orthogonal weave pattern of 0.3 mm diameter Barkley FBA BGQS15–15 nylon monofilament and polyester resin Composite Envisions 1179. Four types of samples were performed with the longitudinal distance between binders of 0.5, 1, 1.5, and 2 cm, respectively, as shown in **Figure 2** and, from now on. These samples will be defined as:

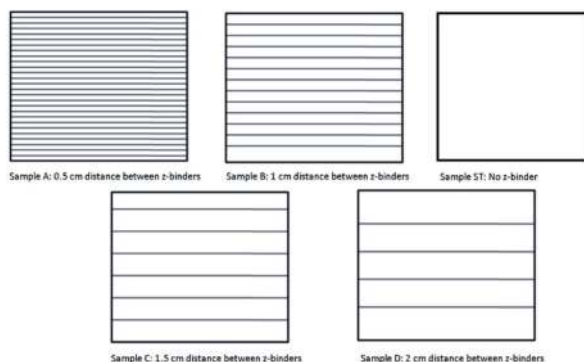


Figure 2. Different samples with the longitudinal distance between binders.

- A: Binder distance of 0.5 cm.
- B: Binder distance of 1 cm.
- C: Binder distance of 1.5 cm.
- D: Binder distance of 2 cm.
- ST: Sample with no binder.

10 specimens from each sample were made and were identified by consecutive numbers, for instance, specimen A1, A2, ... A10 for sample A; B1, B2, ... B10 for samples B, but different issues were presented during tests and in the results section only is shown the results of the most relevant specimens.

The DCB tests per the ASTM D5528 standard were performed on a Sintech 20 D tensile testing machine with a constant crosshead speed equal to 5 mm/min equipped with 50 kN load cell. All test load-displacement data were recorded by Sintech software. To measure all propagation of delamination values, all tests were filmed with a Samsung S20 Ultra camera with a resolution of 4 K/120 fps and processed in Tracker software.

3. Results and discussion

3.1 Delamination test

Figure 3 shows the sequence of a bending mechanism pattern that all specimens with binder had because of the elasticity of the z-axis yarn, improving the toughness of the composite and preventing the delamination from propagating. A “lever” was generated between the force applied and the z-axis binder until the binder fractured.

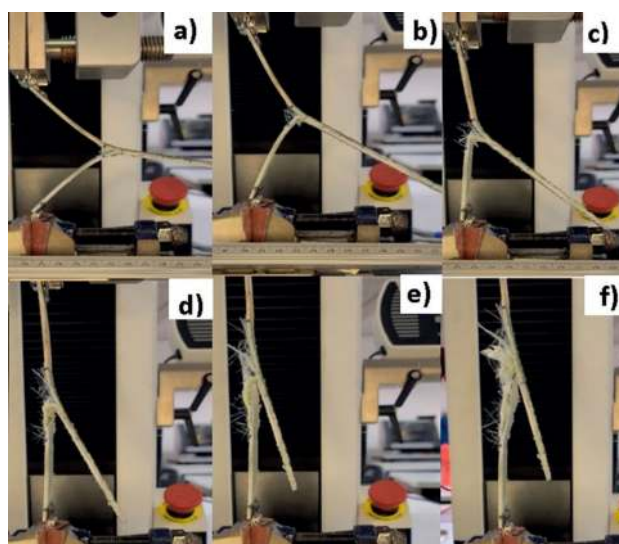


Figure 3.
Sequence of DCB test.

it repeats the same lever mechanism from the next closest binder in a staggered manner until (1) the piano hinge came off, (2) the tensile machine stopped, or (3) the specimen fractured causing this bending a relatively high displacement between layers δ and consequently a destructive tear for the composite.

Figure 4 shows the load-displacement curve resulting from the delamination test, and **Figure 5** shows the R-curve of most representative specimens. Specimen ST6 shows a conventional pattern for delamination composites, with pronounced noise on the Y-axis because the values were too small for the testing machine. The linear pattern indicates detachment of the fibers within the composite due to a premature

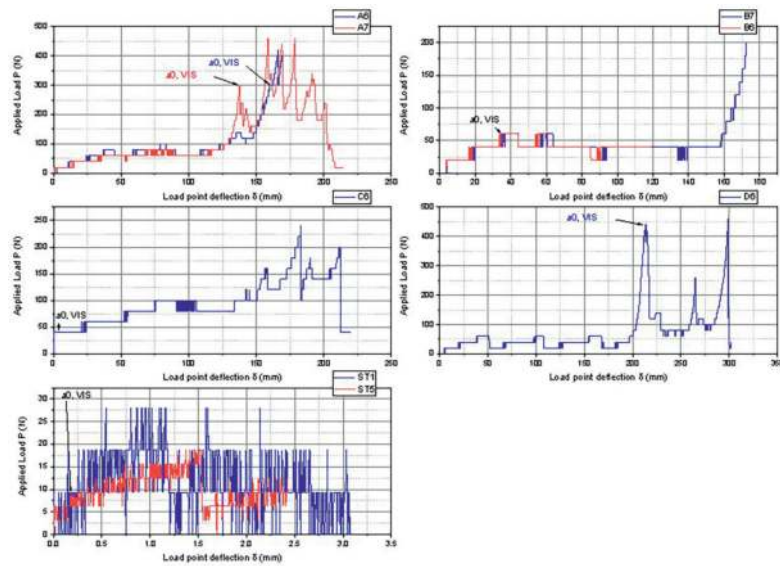


Figure 4.
Load-displacement curve from DCB tests.

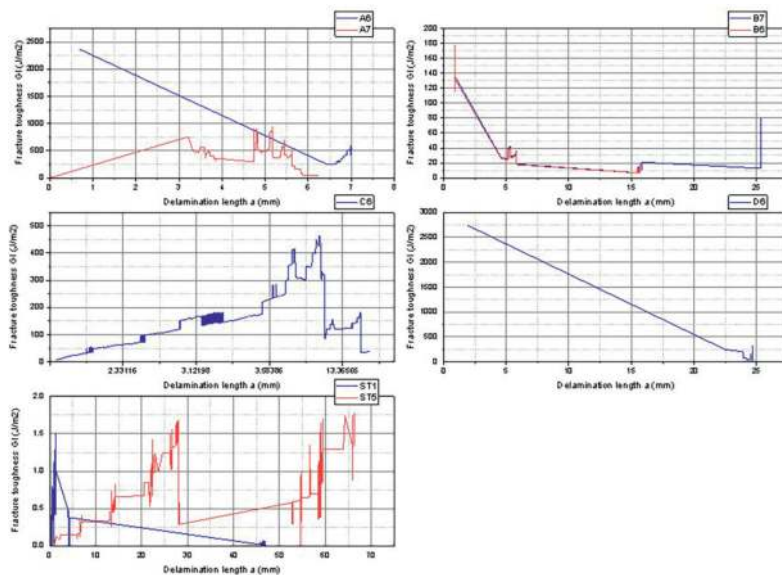


Figure 5.
R curves from DCB tests.

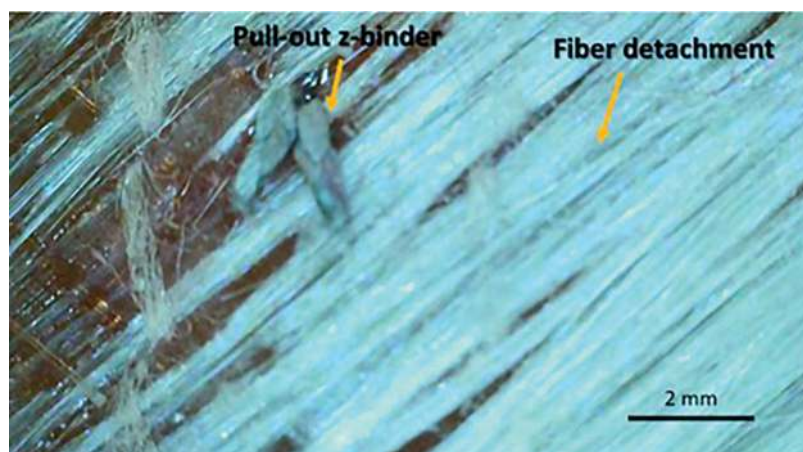


Figure 6.
Pull-out z-binder and fiber detachment.

failure in the matrix. The visible delamination (VIS) starts very early with a very minimal delamination length of “a.” In the curve, 2 peaks stand out that visibly coincide with the delamination from the insert and its propagation.

Specimens A, B, C, and D had a behavior very different from conventional delamination. The beginning of delamination from the “VIS” point of specimens A6, A7, B6, B7, and D6 is highlighted by a very pronounced first peak caused by the rupture of the closest z-binder from the insert. The load decrease while increasing displacement as delamination propagates until it reaches the next z-binder. It will increase the load required to keep delamination crack growing and so on. The nonlinear zones in the curves lie in the plasticity of the z-binder trying to maintain the layers together, and the peaks above represent pull-out fracture, that is, the z-binders fractures plastically and they are pulled out from the matrix. Both fracture mechanisms are illustrated in **Figure 6**. The C6 curve, which also had a premature detachment of one of the piano hinges, shows the same pattern as the previous specimens with a z-binder. The pronounced peaks belong to the ductile fracture of the z-binder and, therefore, pull-out. **Figure 5** shows an intermediate GI value between specimens A and B. Specimen D6 had a similar performance to specimens A6 and A7, with the exception that D6 has fewer peaks due to the distance between the z-binder of 0.5 vs. 2 cm. Both maximum peaks of specimens A and D are close to 20 MPa and due to the greater number of peaks, specimen D has a smaller area under the curve and, therefore, a lower toughness modulus.

Specimens A6 and A7 were the ones that exhibited the highest toughness and maximum stresses in the DCB test specimens B6 and B7 had a premature failure in the joint of the piano hinges. However, **Figure 5** illustrated how the fiber detachment mechanism started with a linear pattern in the curve. The stresses supported were also higher than ST6. **Figures 5** B6 and B7 show that the specimens with z-binder, they had the lowest values of GI toughness. However, higher than that of the specimen without a z-binder.

Figure 7 shows all stress-displacement curves in a single plot, where the difference between them can be seen: The most predominant specimens were A7 and D7 because no issues were found in the tests. Of these 2 specimens, both had maximum stress of 18.74 MPa, but specimen A7 had a higher modulus of toughness than specimen D7, 1.035 J/mm³ vs. 0.885 J/mm³, due to a greater number of peaks that are generated

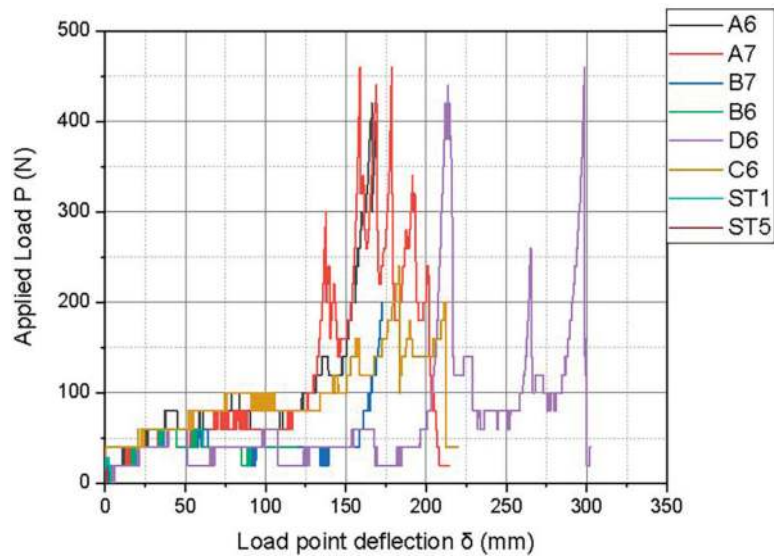


Figure 7.
Load-displacement for all specimens from DCB test.

by the z-binder since it has a smaller distance between them. However, specimen D7 showed a greater displacement than specimen A7 due to the fact the z-binders blocked the latter. Despite all the drawbacks, all the samples with z-binders presented better results than those without them, which is barely visible in **Figure 7** due to their low interlaminar resistance. The instability presented in all the specimens with z-binders falls on the binder itself, where the most witnessed peaks are due to the resistance generated by them, and the pronounced valleys followed by these peaks are the rupture of the z-binders due to ductile fracture.

Table 1 shows the results from load-displacement curves from DCB tests. The specimens that registered a higher resistance against delamination were A7 and D4, with a value of 18.74 MPa ST6 was the one that registered the lowest maximum stress with 0.7 MPa. B and C show intermediate resistance values. Specimen D4 had the largest shell displacement, which for this type of test is a very large value compared to the displacement of 2.42 mm/mm that specimen ST6 had, which is a

Specimens	σ Max (Mpa)	δ @ σ Max (mm)	δ Max (mm)	T J/mm^3	Failure note
ST6	0.7	1.51	2.42	0.00093	Complete delamination
A6	17.11	166.18	168.68	0.651	Specimen fractures
A7	18.74	158.76	213	1.035	Specimen fractures
B6	2.44	59.1	123.92	0.193	Piano hinge failure
B7	8.15	172.44	172.44	0.308	Tensile machine stop
C6	9.77	182.9	213.66	0.839	Piano hinge failure
D6	18.74	298.52	302.28	0.885	Specimen fractures

Table 1.
Load-displacement values from DCB test.

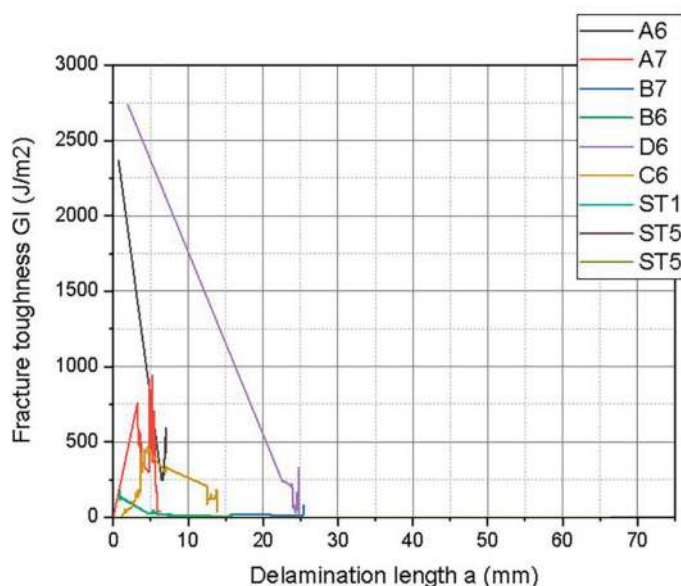


Figure 8.
 Curve R for all specimens from the DCB test.

normal value [33–35]. A7 had the highest tenacity modulus, followed by specimens D6 and C6, with values of 1.035, 0.885, and 0.839 J/mm³, respectively.

Figure 8 shows all R-curves from the DCB test, where A6, A7, and D6 stand out. ST6 (at the bottom of the plot) shows the most delamination width because it was the only specimen to delaminate completely. Despite this, the illustrated toughness is very low compared to the other specimens.

In **Table 2**, the critical values of GI toughness are shown. The high values for A6 and D6 are due to the initial “peak” that was generated to break the first z-binder, and the very low value of ST6 was because delamination was progressive. There was no reinforcement on the interlaminar plane.

3.2 Tensile test

Figure 9 shows the stress-displacement curves of the tensile tests. The linear and semi-linear zones shown in the curves are repeated in these tests, and the mechanism

Specimens	P (N)	δ (mm)	a (mm)	GI _{Max} (J/m ²)
A6	180	152.08	0.68	2367.01
A7	300	137.58	3.2139	758.4
B6	60	44.04	0.88	175.94
B7	60	44.24	0.88	176.49
C6	40	3.5	1.1	7.69
D6	420	17.11	1.93	2733.83
ST6	3.1179	0.0021	0.72	0.00004

Table 2.
 Delamination values from DCB test.

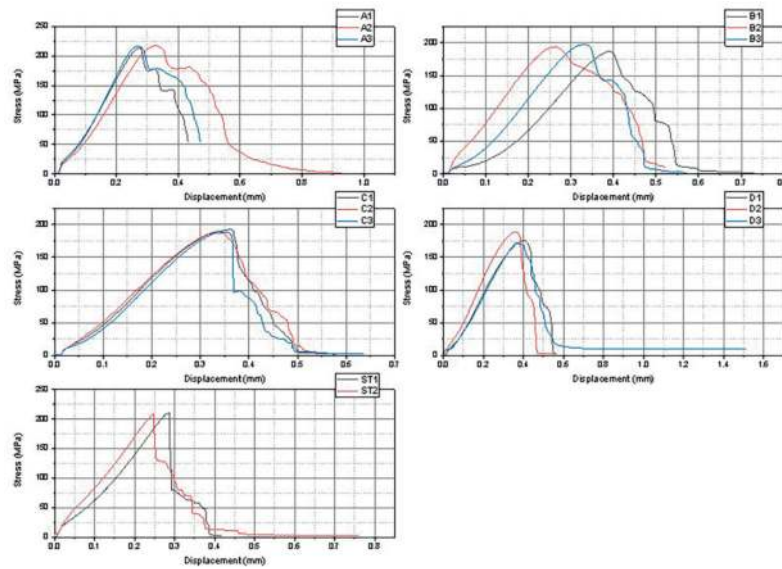


Figure 9.
Stress-displacement curves from tensile tests.

Specimens	UTS Mpa	E GPa	σ_y (2%) MPa	ϵ @ σ_y mm/ mm	U_R MJ/ m^3	T J/ mm^3	ϵ Max mm/ mm	SE %
A	215.79	0.96	198.95	0.25	22.46	0.061	0.48	1.92
B	192.6	0.82	180.77	0.29	22.05	0.05	0.48	3.12
C	189.37	0.72	165.48	0.27	20.13	0.045	0.44	1.34
D	178.58	0.61	157.85	0.3	21.84	0.049	0.49	4.96
ST	209.63	0.85	208.89	0.26	25.97	0.035	0.37	0.8

Table 3.
Values obtain from tensile test.

was the same as in the delamination tests. Linear zones are because of matrix cracking within the composite, and nonlinear zones because of the fibers' pull-out mechanism and the elasticity of z-binders within the composite. In **Table 3** the mechanical properties of the tensile tests are listed. Sample A has the maximum value of the UTS close to ST. Then the UTS value decreases because z-binders tend to restrain the fibers making the composite weaker, the distance between z-binders is even stronger at some point (sample A), the lesser the distance. The modulus of toughness increases on the samples with z-binder, mainly because the z-binder makes the composite absorb more energy than sample ST.

3.3 Fracture analysis

Due to the complexity of the different failure mechanisms, the specimens presented in the delamination test, the analysis was divided into 3 zones, as shown in **Figure 10**. Zone A is located in the interlaminar fracture zone where delamination occurs, Zone B is the flexural zone of the composite previously explained, and Zone C is the zone of collateral damage, where residual stresses are generated due to Zone B.

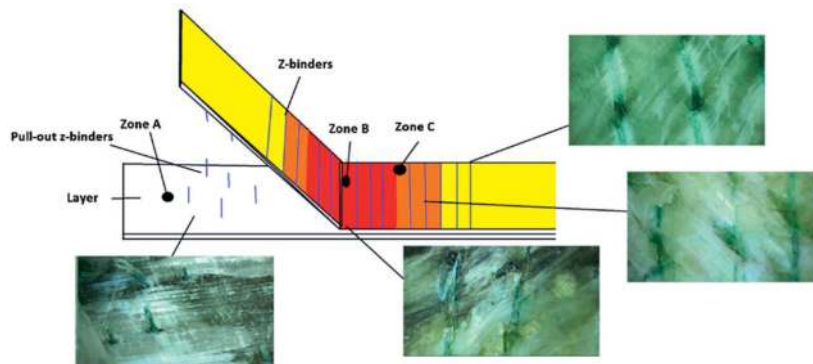


Figure 10.
Scheme of failure mechanism zones in DCB test.

3.3.1 Zone A

Interlaminar fracture failure in this zone results from the composite insert according to ASTM D5528 and shows similar fracture patterns in all tests with z-binder. The ST specimens, shown in **Figure 11**, were completely delaminated. It shows an interlaminar brittle fracture, where islands of exposed fiber were found without matrix, since in some areas the matrix fractured, leaving exposed fibers. No fiber fracture was found. In

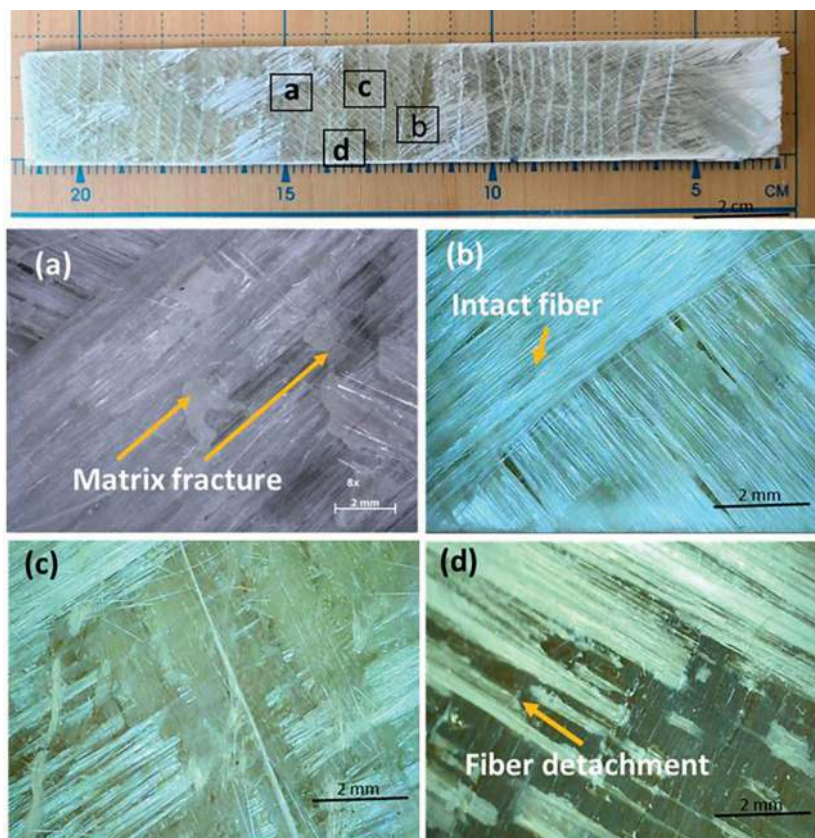


Figure 11.
Fracture mechanism in ST specimens.

Figure 11c some “whitish” areas were generated because of fibers’ detachment within the composite, due to internal matrix fracture, which are presented in all 3 zones.

In the case of specimens A, B, C, and D, there were various additional mechanisms to those that occurred in the ST specimen regarding delamination, as shown in **Figure 12**. Due to its nature, The z-binder shows a ductile pull-out fracture, and the filament is made of nylon. However, close to z-binders, no damage to the fibers was found. There are also fibers exposed because of brittle matrix failure. Something very relevant is shown in **Figure 12c**, where the z-binder shows a cavity in the form of residual stress concentrators that will affect the material resistance in a direction perpendicular to the fibers. A “fiber bridging” effect from z-binders was responsible for the improvement of interlaminar fracture toughness for Zone B.

3.3.2 Zone B

This area was the most affected due to the z-binder. **Figure 13** shows as the z-binder prevent the propagation of the interlaminar fracture due to its elasticity. The composite reaction in the test was to bend the upper layer, conglomerate the fibers and the z-binders in the flexing zone, and generate a hardening in the specimens as z-binders fracture progressively across the composite generating a greater flexing and at the same time a lock in the plane. These bending fractures the matrix, detaching

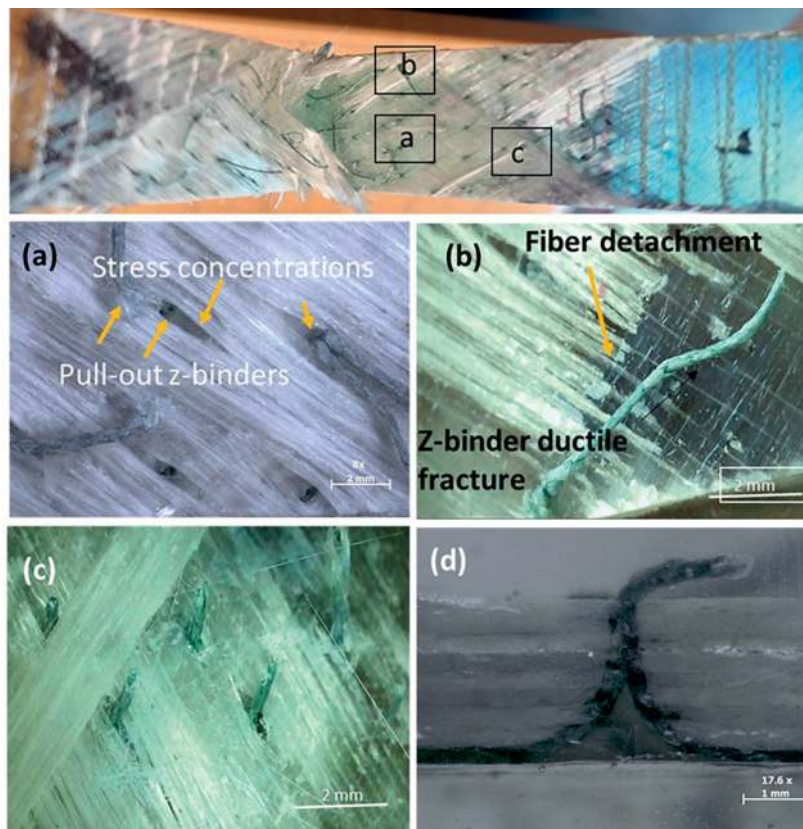


Figure 12.
Zone A, fracture mechanism in z-binder specimens.

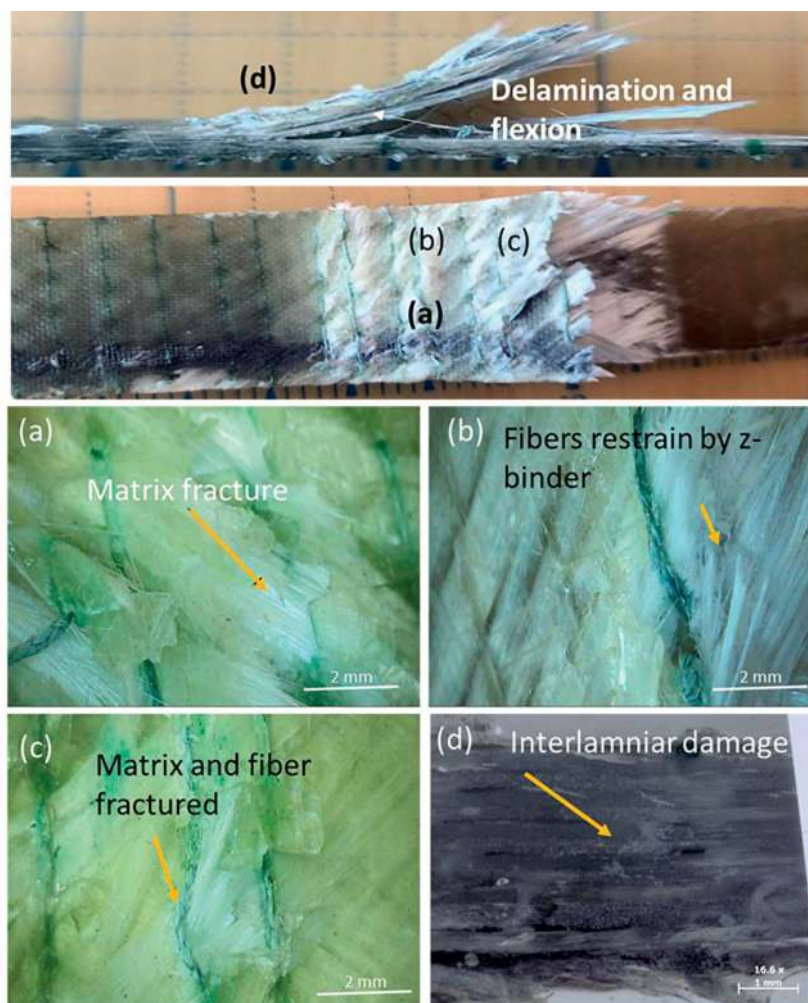


Figure 13.
Zone B fracture mechanism in z-binder specimens.

the fiber as Zone A. The fracture mechanism in the detached fibers is generated since z-binders generate “knots” within the fiber, limiting the pull-out effect, hardening and embrittling the material to a point where the fibers begin to fracture due to the flexural stress generated. Additionally, delamination was found as a collateral effect due to the bending in the upper layer of the composite (where the stress is applied).

3.3.3 Zone C

As shown in **Figure 14**, this zone is the result of the propagation of the stresses generated in Zone B, distributing energy in the fibers and z-binders, generating stress concentrators. Here prevail the “whitish” zones previously explained, where a superficial fracture of the matrix was found in some zones. This zone is generated as collateral damage from Zone B since the energy absorbed is too much for the matrix. Z-binders knots were also creating the whitish zones. **Figure 14c** and **d** show that there is interlaminar damage.

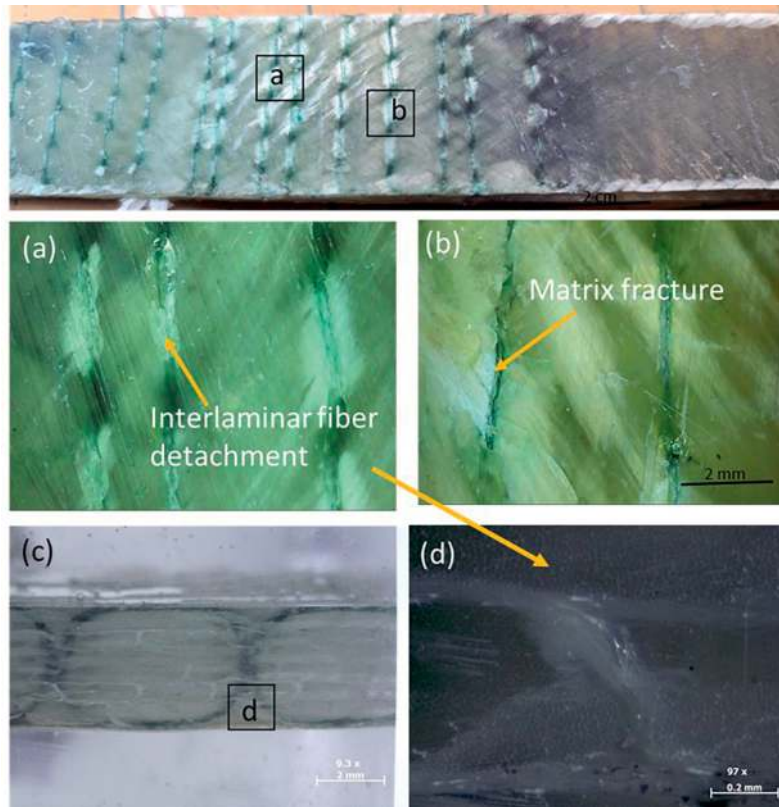


Figure 14.
Zone C fracture mechanism in z-binder specimens.

3.3.4 Tensile test fracture

Figure 15 illustrates the tensile test fracture of one sample specimen, which was angled fracture (Angle- Gauge- Middle, AGM, according to ASTM D3039 standard) with “pull-out” failure. **Figure 16** shows that all specimens had delamination. The fracture mechanisms on all z-binder specimens are shown in **Figures 17 and 18**, the layers were displaced by the tensile force and “pull-out” failure, damaging the z-binder, which were tied to the layers themselves, generating stress concentrators, fractures in the matrix and delamination. In samples “A” and “B” multiple fractures on the fibers were found because z-binders prevent their displacement and, therefore, fracture. In samples “C” and “D”, the composite damage due to the z-binder is less, reducing the fracture in the fibers and the matrix in the region close to the failure.

Z-binder on 3D composites may generate collateral damage reducing mechanical properties such as compression [36–43] and/or flexural resistance [44–51]. This is mainly because such composites’ manufacturing may generate resin-rich zones that can fracture prematurely and start different fracture mechanisms that depend on z-binder configuration and nature. Even though, due to their promising properties, 3D composites are of great interest for replacing metals applications, with different advantages such as corrosion resistance [52–56]. This motivates the generation of novel manufacturing processes such as the one presented in this study, a zigzag-oriented z-binder [57], or even a 2.5D pattern composite [58].

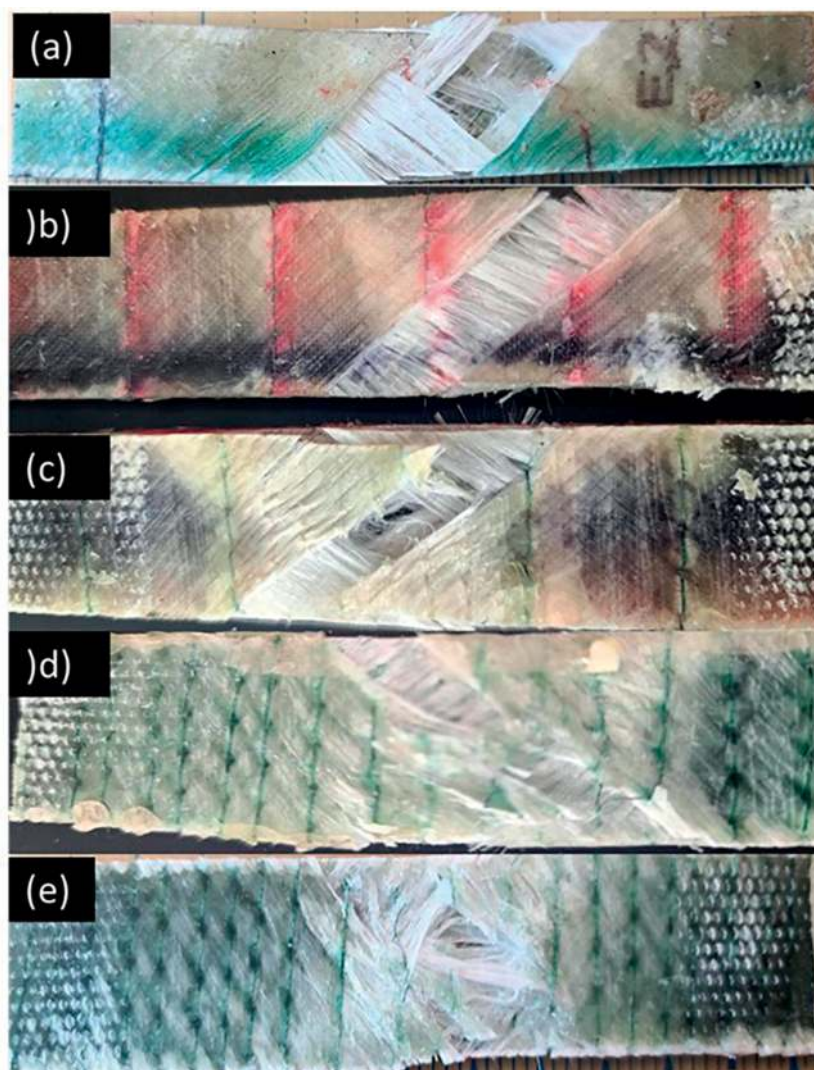


Figure 15.
Fractures of the samples tested by tension: a) ST, b) A, c) B, d) C, e) D.

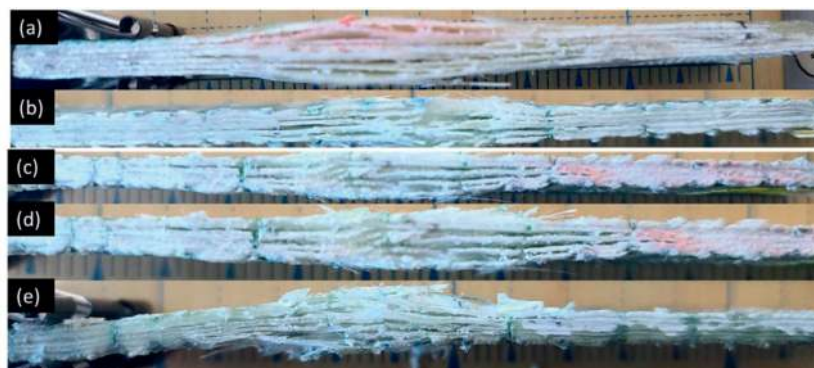


Figure 16.
Fractures in cross section of the samples tested by tension: a) ST, b) A, c) B, d) C, e) D.

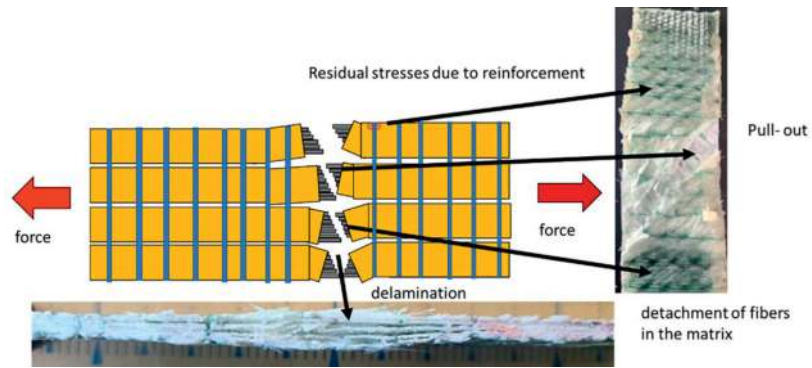


Figure 17.
Fracture mechanisms in tension test.

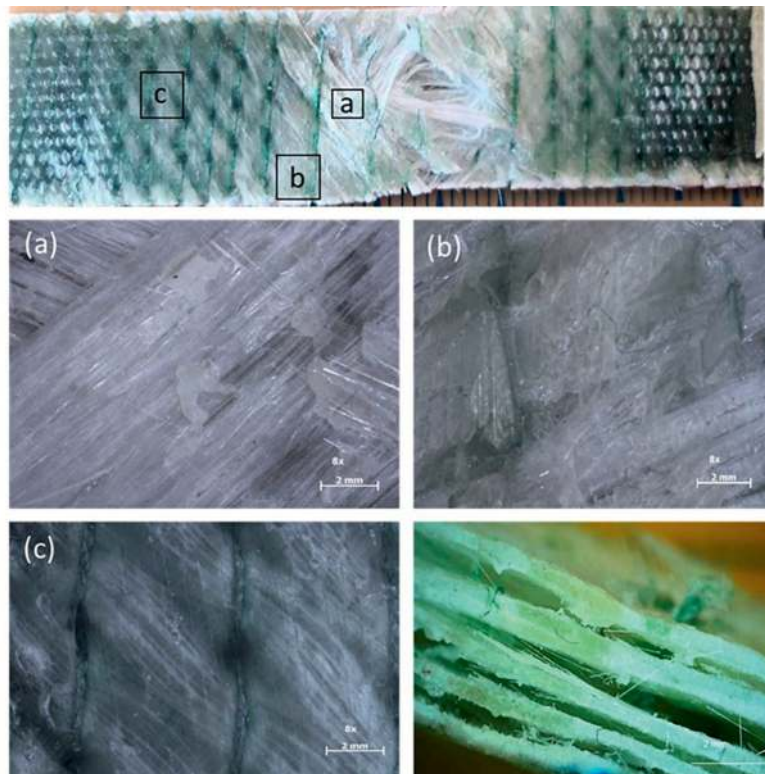


Figure 18.
Tensile fracture morphology.

4. Conclusions

Four fiberglass/polyester composite samples with different thin nylon z- binder reinforce lengths were tested. All samples showed an increase in mode 1 interlaminar fracture toughness over the same composite without a z-binder, but a new fracture mechanism also appears because of the elasticity of the z-binder and brittle matrix. Tensile tests were also made, and results show that tensile resistance in samples B, C, and D been compromised. Sample A had a small increase in tensile resistance, showing that the lesser the length distance between z-binder, the better tensile resistance.

All these results showed promising values. More studies need to be made on z-binder length distance smaller than 0.5 mm since Sample A had the best properties overall. Also, a matrix with superior mechanical properties than the z-binder reinforcement is recommended, since the new fracture mechanism was created because the matrix was weaker than the z-binder. With this, better values shall result.

Nomenclature

P	Applied load (N)
G_I	Opening Mode I interlaminar fracture toughness (J/m^2)
a_0	Interlaminar delamination length (mm)
VIS	Point at which delamination is observed visually on specimen edge
δ	Load point deflection, mm
b	width of DCB specimen, mm (25.4 mm)
a	Delamination length, mm
UTS	Ultimate tensile strength (MPa)
E	Modulus of elasticity (GPa)
σ_y (2%)	Yield strength at 2% (MPa)
$\epsilon @ \sigma_y$	Displacement at yield strength (mm/mm)
UR	Modulus of resilience (MJ/m^3)
T	Modulus of toughness (J/mm^3)
SE	Standard error of the mean (%)

Author details

Citlalli Gaona-Tiburcio^{1*}, Alejandro Lira-Martínez², Marianggy Gomez-Avila², Jesús M. Jaquez-Muñoz¹, Miguel Angel Baltazar-Zamora³, Laura Landa-Ruiz³, Demetrio Nieves-Mendoza³, Francisco Estupiñan-López¹ and Facundo Almeraya-Calderón¹


1 Universidad Autónoma de Nuevo León, UANL, Facultad de Ingeniería Mecánica y Eléctrica, FIME, Centro de Investigación e Innovación en Ingeniería Aeronáutica, CIIIA, Aeropuerto Internacional del Norte, Nuevo León, México

2 Universidad Autónoma de Ciudad Juárez. Instituto de Ingeniería y Tecnología, Chihuahua. México

3 Facultad de Ingeniería Civil-Xalapa, Universidad Veracruzana, Veracruz, Mexico

*Address all correspondence to: citlalli.gaona@gmail.com

IntechOpen

© 2022 The Author(s). Licensee IntechOpen. This chapter is distributed under the terms of the Creative Commons Attribution License (<http://creativecommons.org/licenses/by/3.0>), which permits unrestricted use, distribution, and reproduction in any medium, provided the original work is properly cited. 

References

- [1] Abramovich H. Stability and Vibrations of Thin/Walled Composite Structures. 1st ed. Cambridge, United Kingdom: Woodhead Publishing; 2017
- [2] Mouritz A. Introduction to Aerospace Materials. 1st ed. Cambridge, United Kingdom: Woodhead Publishing; 2012
- [3] Wisnom W. The Role of Delamination in Failure of Fibre-Reinforced Composites. 1st ed. London, England: The Royal Society Publishing; 2012
- [4] Bagherpour S. Fibre reinforced polyester composites. In: Polyester. London, United Kingdom: IntechOpen; 2012. DOI: 10.5772/48697
- [5] Gupta M. Investigations on properties of glass fibre reinforced polymer composite. American Journal of Polymer Science & Engineering. 2018;6:5-8
- [6] Ganjiani M, Safarabadi M. Effects of delamination in drilling glass/polyester composite. Frontiers of Structural and Civil Engineering. 2021;15:552-567. DOI: 10.1007/s11709-021-0699-7
- [7] Triki E, Zouari B, Abdessalem J, Fakhreddine D. Experimental investigation of the Interface behavior of balanced and unbalanced E-glass/polyester woven fabric composite laminates. Applied Composite Materials. 2013;20:1111-1123. DOI: 10.1007/s10443-013-9322-y
- [8] Sham M, Venkatesha C, Jayaraju T. Experimental methods of determining fracture toughness of Fiber reinforced polymer composites under various loading conditions. Journal of Minerals and Materials Characterization and Engineering. 2011;10:1-9. DOI: 10.4236/jmmce.2011.1013099
- [9] Khoramshahi A, Choupani N. Influence of mixed-mode ratio on delamination fracture toughness and energy release rate of glass/polyester laminates. Key Engineering Materials. 2011;471-472:874-879. DOI: 10.4028/www.scientific.net/KEM.471-472.874
- [10] Suriani MJ, Rapi HZ, Ilyas RA, Petrú M, Sapuan SM. Delamination and manufacturing defects in natural Fiber-reinforced hybrid composite: A review. Polymers. 2021;13:1323. DOI: 10.3390/polym13081323
- [11] Zhou H, Du X, Liu H, Zhang Y, Mai Y. Delamination toughening of carbon fiber/epoxy laminates by hierarchical carbon nanotube-short carbon fiber interleaves. Composites Science and Technology. 2017;140:46-53. DOI: 10.1016/j.compscitech.2016.12.018
- [12] Ou Y, González C, Vilatela J. Understanding interlaminar toughening of unidirectional CFRP laminates with carbon nanotube veils. Composites Part B: Engineering. 2020;201. DOI: 10.1016/j.compositesb.2020.108372
- [13] Kuwata M, Hogg P. Interlaminar toughness of interleaved CFRP using non-woven veils: Part 1. Mode-I testing. Composites Part A: Applied Science and Manufacturing. 2011;42:1551-1559. DOI: 10.1016/j.compositesa.2011.07.016
- [14] Hamer S, Leibovich H, Green A, Intrater R, Avrahami R, Zussman E, et al. Mode I interlaminar fracture toughness of Nylon 66 nanofibrillated interleaved carbon/epoxy laminates. Polymer Composites. 2011;32:1781-1789. DOI: 10.1002/pc.21210
- [15] Yasae M, Bond I, Trask R, Greenhalgh E. Mode I interfacial

toughening through discontinuous interleaves for damage suppression and control. *Composites Part A: Applied Science and Manufacturing*. 2012;**43**:198-207. DOI: 10.1016/j.compositesa.2011.10.009

[16] Zheng N, Huang Y, Liu H, Gao J, Mai Y. Improvement of interlaminar fracture toughness in carbon fiber/epoxy composites with carbon nanotubes/polysulfone interleaves. *Composites Science and Technology*. 2017;**140**:8-15. DOI: 10.1016/j.compscitech.2016.12.017

[17] Saz-Orozco B, Ray D, Stanley W. Effect of thermoplastic veils on interlaminar fracture toughness of a glass fiber/vinyl ester composite. *Polymer Composites*. 2017;**38**:2501-2508. DOI: 10.1002/pc.23840

[18] Kim J, Sham M. Impact and delamination failure of woven-fabric composites. *Composites Science and Technology*. 2000;**60**:745-761. DOI: 10.1016/S0266-3538(99)00166-9

[19] Rugg KL, Cox BN, Massabo R. Mixed mode delamination of polymer laminates reinforced through the thickness by z-fibres. *Composites Part A Applied Science and Manufacturing*. 2002;**33**:177-190

[20] Sridhar N, Massabo R, Cox BN. Delamination dynamics in through thickness reinforced laminates with application to DCB specimen. *International Journal of Fracture*. 2002;**118**(2):119-144

[21] Yan W, Liu H-Y, Mai Y-W. Numerical study on the mode I delamination toughness of z-pinned laminates. *Composites Science and Technology*. 2003;**63**:1481-1493

[22] Igelmo G. Análisis de la fractura interlaminar en modo I de laminados

unidireccionales y angulares. Bilbao: Universidad del País Vasco; 2017

[23] Saleh M, Soutis C. Recent advancements in mechanical characterization of 3D woven composites. *Mechanics of Advanced Materials and Modern Processes*. 2017;**3**(12):1-17. DOI: 10.1186/s40759-017-0027-z

[24] Ostrower J. Delamination Prompts Boeing to Inspect 787 Fleet [Internet]. 2021. Available from: <https://www.flightglobal.com/delamination-prompts-boeing-to-inspect-787-fleet/103901>. article

[25] Liu H-Y, Mai Y-W. Effect of z-pin reinforcement on interlaminar mode I delamination. In: Zhang Y, editor. *Proceedings of ICCM13*. Beijing, China. 2001

[26] Safran. Leap 1-A Engine [Internet]. 2022. Available from: <https://www.safran-group.com/products-services/leap-1a-new-generation-engine-single-aisle-commercial-jets>

[27] ASTM. D3039-00; Standard Test Method for Tensile Properties of Polymer Matrix Composite Materials. West Conshohocken, PA, USA: ASTM International; 2000

[28] ASTM. D5528-21; Standard Test Method for Mode I Interlaminar Fracture Toughness of Unidirectional Fiber-Reinforced Polymer Matrix Composites. West Conshohocken, PA, USA: ASTM International; 2021

[29] Mouritz AP. Review of z-pinned laminates and sandwich composites. *Composites Part A: Applied Science and Manufacturing*. 2020;**106**:128:1-44. DOI: 10.1016/j.compositesa.2020.106128

[30] Australian Transport Safety Bureau. *Trailing Edge Flap Delamination*

- Involving a Boeing 737-800, near Gold Coast Airport, Qld, on 19 January 2020 [Internet]. 2020. Available from: <https://www.atsb.gov.au/publications/occurrence-briefs/2020/aviation/ab-2020-006/>
- [31] Ostrower J. Boeing pulls eight 787s from service over structural issues. 2020. Available from: <https://theaircurrent.com/aviation-safety/boeing-pulls-eight-787s-from-service-over-structural-issue/>
- [32] Charlie H. Report raises new questions about structural integrity of Boeing 787 Dreamliner. 2020. Available from: <https://komonews.com/news/local/report-raises-new-questions-about-structural-integrity-of-boeing-787-dreamliner>
- [33] Bashar MT, Sundararaj U, Mertiny P. Dependence of fracture toughness of composite laminates on interface ply orientations and delamination growth direction. *Composite Science*. 2004;**64**:2139-2152
- [34] Ozdil F, Carlsson L. Beam analysis of angle-ply laminate DCB specimens. *Science*. 1999;**59**:305-315
- [35] Shokrieh M, Zeinedini A. Delamination R curve as a material property of unidirectional glass/epoxy composite. *Composite Materials*. 2012;**34**:211-218
- [36] Cox B, Dadkhah M, Inman R, Morris W, Zupon J. Mechanisms of compressive failure in 3D composites. *Acta Metallurgica et Materialia*. 1992;**40**:3285-7151. DOI: 10.1016/0956-7151(92)90042-D
- [37] Kuo W, Ko T. Compressive damage in 3-axis orthogonal fabric composites. *Composites Part A: Applied Science and Manufacturing*. 2000;**31**:1091-1105. DOI: 10.1016/S1359-835X(00)00066-X
- [38] Kuo W, Ko T, Chen C. Effect of weaving processes on compressive behavior of 3D woven composites. *Composites Part A: Applied Science and Manufacturing*. 2007;**38**:555-565. DOI: 10.1016/j.compositesa.2006.02.025
- [39] Zhou G, Davies G. Characterization of thick glass woven roving/polyester laminates: 1. Tension, compression, and shear. *Composites*. 1995;**26**:579-586. DOI: 10.1016/0010-4361(95)92622-J
- [40] Zheng T, Guo L, Sun R, Li Z, Yu H. Investigation on the compressive damage mechanisms of 3D woven composites considering stochastic fiber initial misalignment. *Composites Part A: Applied Science and Manufacturing*. 2021;**143**:1-13. DOI: 10.1016/j.compositesa.2021.106295
- [41] Guo Q, Zhang Y, Li D, Sun X, Li M, Li C. Experimental characterization of the compressive properties and failure mechanism of novel multiaxial 3D woven composites. *Composites Communications*. 2021;**28**:1-6. DOI: 10.1016/j.coco.2021.100905
- [42] Guo J, Ke Y, Wu Y, Gu B, Sun B. Effects of defect sizes at different locations on compressive behaviors of 3D braided composites. *Thin-Walled Structures*. 2022;**179**:1-13. DOI: 10.1016/j.tws.2022.109563
- [43] Jin L, Niu Z, Jin B, Sun B, Gu B. Comparisons of static bending and fatigue damage between 3D angle-interlock and 3D orthogonal woven composites. *Journal of Reinforced Plastics and Composites*. 2012;**31**(14):935-945. DOI: 10.1177/0731684412450626
- [44] Kuo W. The role of loops in 3D fabric composites. *Composites Science and Technology*. 2000;**60**:1835-1849. DOI: 10.1016/S0266-3538(00)00075-0

- [45] Adanur S, Tam C. On-machine interlocking of 3D laminate structures for composites. *Composites Part B: Engineering*. 1997;**28**:497-506. DOI: 10.1016/S1359-8368(96)00084-4
- [46] Jia X, Xia Z, Gu B. Numerical analyses of 3D orthogonal woven composite under three-point bending from multi-scale microstructure approach. *Computational Materials Science*. 2013;**79**:468-477. DOI: 10.1016/j.commatsci.2013.06.050
- [47] Li D, Zhao C, Jiang L, Jiang N. Experimental study on the bending properties and failure mechanism of 3D integrated woven spacer composites at room and cryogenic temperature. *Composite Structures*. 2014;**111**:56-65. DOI: 10.1016/j.compstruct.2013.12.026
- [48] Turner P, Liu T, Zeng X. Collapse of 3D orthogonal woven carbon fibre composites under in-plane tension/compression and out-of-plane bending. *Composite Structures*. 2016;**142**:286-297. DOI: 10.1016/j.compstruct.2016.01.100
- [49] Zhang D, Sun M, Liu X, Xiao X, Qian K. Off-axis bending behaviors and failure characterization of 3D woven composites. *Composite Structures*. 2019;**208**:45-55. DOI: 10.1016/j.compstruct.2018.10.009
- [50] Fan W, Dong J, Wei B, Zhi C, Yu L, Xue L, et al. Fast and accurate bending modulus prediction of 3D woven composites via experimental modal analysis. *Polymer Testing*. 2019;**78**:1-6. DOI: 10.1016/j.polymertesting.2019.105938
- [51] Cartie DDR. *Effect of Z-Fibre™ on the Delamination Behaviour Carbon/Epoxy Laminates*. Cranfield, United Kingdom: Cranfield University; 2000
- [52] Gaona-Tiburcio C, Ramirez A, Gonzalez-Rodriguez J, Campillo B. An Electrochemical Study of the Corrosion Behavior of a Dual Phase Steel in 0.5M H₂SO₄. *International Journal of Electrochemical Science*. 2010:1786
- [53] Nanjan S, Murali JG. Analysing the mechanical properties and corrosion phenomenon of reinforced metal matrix composite. *Materials Research*. 2020;**23**(2):e20190681
- [54] Martínez-Villafañe A, Almeraya-Calderón F, Gaona-Tiburcio C, Gonzalez-Rodriguez J. Porcayo-Calderón. *Journal of Materials Engineering and Performance*. 1998;**7**:108-113
- [55] Bodunrin MO, Alaneme KK, Chown LH. Aluminium matrix hybrid composites: A review of reinforcement philosophies; mechanical, corrosion and tribological characteristics. *Journal of Materials Research and Technology*; **14**(4):434
- [56] Almeraya- Calderon F, Montoya-R M, Garza-Montes-de-Oca N, Castorena J, Estupiñan- Lopez F, Miramontes J, et al. Corrosion behavior of multilayer coatings deposited by PVD on Inconel 718 in chloride and sulphuric acid solutions. *International Journal of Electrochemical Science*. 2019;**14**:9596-9609. DOI: 10.20964/2019.10.45
- [57] Hu Q, Memon H, Qiu Y, Wei Y. The failure mechanism of composite stiffener components reinforced with 3D woven fabrics. *Materials (Basel)*. 2019;**12**:1-17. DOI: 10.3390/ma12142221
- [58] Zhu L, Lyu L, Zhang X, Wang Y, Guo J, Xiong X. Bending properties of zigzag-shaped 3D woven spacer composites: Experiment and FEM simulation. *Materials (Basel)*. 2019;**12**: 1-11. DOI: 10.3390/ma12071075